ACS APPLIED MATERIALS & INTERFACES

www.acsami.org

Research Article

Development of Hybrid Pseudohalide Tin Perovskites for Highly Stable Carbon-Electrode Solar Cells

Mohammad Rameez, Eric Yan-Ru Lin, Putikam Raghunath, Sudhakar Narra, Donghoon Song, Ming-Chang Lin, Chen-Hsiung Hung,* and Eric Wei-Guang Diau*

Cite This: https://dx.doi.org/10.1021/acsami.0c03704

Read Online

ACCESS | Metrics & More | Article Recommendations | Supporting Information

ABSTRACT: Tin-based perovskites degrade rapidly upon interaction with water and oxygen in air because Sn−I bonds are weak. To address this issue, we developed novel tin perovskites, $FASnI_{(3-x)}(SCN)_x$ (x = 0, 1, 2, or 3), by employing a pseudohalide, thiocyanate (SCN^-), as a replacement for halides and as an inhibitor to suppress the Sn^{2+}/Sn^{4+} oxidation. The structural and electronic properties of pseudohalide tin perovskites in this series were explored with quantum-chemical calculations by employing the plane-wave density functional theory (DFT) method; the corresponding results are consistent with the experimental results. Carbon-based perovskite devices fabricated with tin perovskite $FASnI(SCN)_2$ showed about a threefold enhancement of the device efficiency (2.4%) relative to that of the best $FASnI_3$-based device (0.9%), which we attribute to the improved suppression of the formation of Sn^{4+}, retarded charge recombination, enhanced hydrophobicity, and stronger interactions between Sn and thiocyanate for $FASnI(SCN)_2$ than those for $FASnI_3$. After the incorporation of phenylethyleneammonium iodide (PEAI, 10%) and ethylenediammonium diiodide ($EDAI_2$, 5%) as coadditives, the $FASnI(SCN)_2$ device gave the best photovoltaic performance with J_{SC} = 20.17 mA cm^{-2}, V_{OC} = 322 mV, fill factor (FF) = 0.574, and overall efficiency of power conversion PCE = 3.7%. Moreover, these pseudohalide-containing devices display negligible photocurrent−voltage hysteresis and great stability in ambient air conditions.

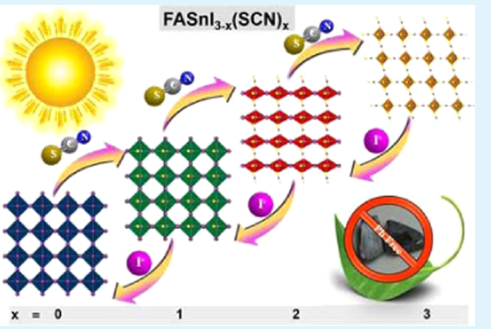

KEYWORDS: *perovskite, pseudohalide, solar cells, tin perovskite, thiocyanate*

INTRODUCTION

Perovskite solar cells (PSC) are rapidly emerging as a front runner for a scalable, cheap, and sustainable energy source with a power conversion efficiency (PCE) surging up to ∼25%,[1] which is comparable with that of the conventional Si solar cells. Nevertheless, for commercialization, it is recommended to replace lead with a less harmful element. Diverse alternative perovskite materials have been explored on adopting tin, copper, germanium, bismuth, or antimony.[2,3] In view of an increased PCE, benefiting from a broad spectrum of light absorption, superior absorption coefficient, and increased charge-carrier mobility, tin perovskites are highly appealing among all lead-free PSC alternatives and are applicable to other optoelectronic devices, e.g., light-emitting diodes, photodetectors, lasers, and transistors.[4,5]

Although tin perovskites exhibit excellent optoelectronic properties, they still suffer from intrinsic defects derived from increased pinholes, many grain boundaries, Sn vacancies, and oxidation of Sn^{2+} to Sn^{4+}.[6] These defects cause intensive hole doping, leading to rapid recombination of charge carriers or a short-circuit of the devices.[7] These effects necessitate their repair on tailoring tin perovskites through the introduction of additives and appropriately selected cations or halides.[8−11] Recent computational results on Sn perovskites have indicated that the Sn−X bond is the most susceptible to the presence of water and oxygen, resulting in instability in an Sn-based PSC.[12] Hence, increasing the hydrophobicity and replacing iodine with moisture-tolerant anions can be suitable approaches for increased efficiencies. Despite the realization of X-site anions in stabilizing Sn perovskites against metal oxidation and retarding charge recombination, little work has been done in this direction. Polyatomic pseudohalides, e.g., thiocyanate (SCN^-) and azide (N_3^-), have been adopted to serve as alternatives for the X-site halides in organic−inorganic hybrid lead perovskites.[13−17] The pseudohalide SCN^- possesses a rigid linear structure and a π-conjugated electronic system beneficial to enhancing the photoelectron transfer.[18] Several reports have described the incorporation of SCN^- as an additive in $MAPbI_3$ PSC devices, demonstrating improved stability and decreased hysteresis. Pseudohalide SCN^- improves moisture tolerance and device stability, decreases trap-assisted recombination, and

Received: February 28, 2020
Accepted: April 16, 2020
Published: April 16, 2020

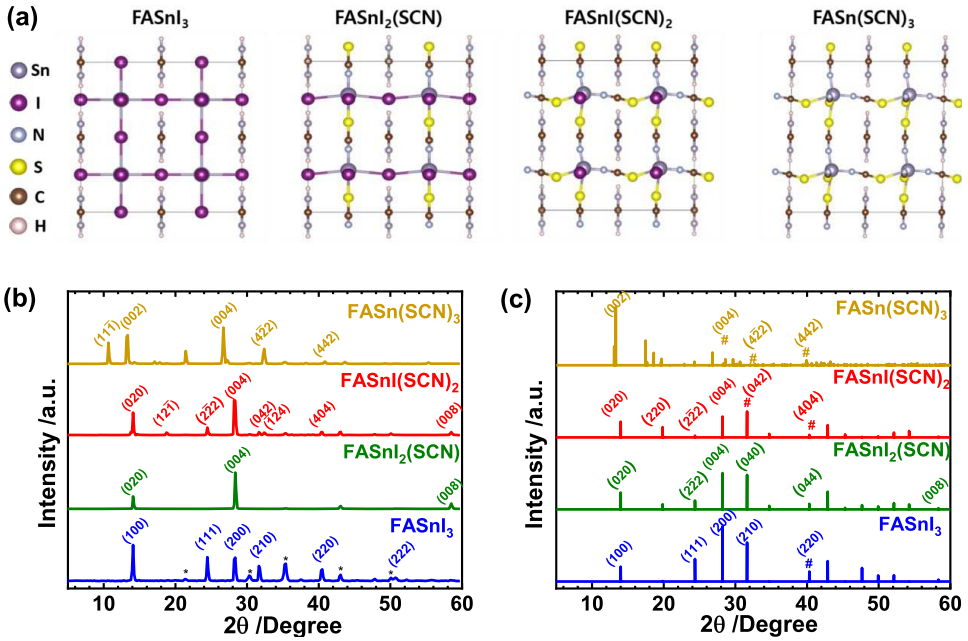

Figure 1. (a) Simulated crystal structure of $FASnI_{(3-x)}(SCN)_x$ (x = 0−3) showing that a three dimensional network is formed by corner-sharing SnX_6 octahedra with FA^+ occupying the interstitial voids. (b) Experimental X-ray diffraction (XRD) patterns of $FASnI_{(3-x)}(SCN)_x$ thin films on an ITO substrate showing the corresponding characteristic signals. Asterisks "*" label the diffraction signals of ITO. (c) Simulated XRD patterns of a $FASnI_{(3-x)}(SCN)_x$ film using crystallographic information converted from (a). The "#" indicates the weak intensity of the diffraction signals.

enhances charge-carrier lifetimes.[13,14,17,19−21] For Pb perovskites, the incorporation of thiocyanates by more than 15% into the lattice, however, leads to the formation of a two-dimensional (2D) structure or mixed phases of $MAPbI_3$ and $MAPbI_2(SCN)$, with $MAPbI_3$ being the dominant phase.[22,23] Pure 2D phase $MA_2Pb(SCN)_2I_2$ exhibits a poor device performance with PCE consistently less than 3.5%.[13,20] In contrast, when used as an additive, thiocyanate-doped Sn perovskite films showed an improved morphology and crystallinity.[4,24] Considering the size difference between Pb^{2+} and Sn^{2+}, we expect the incorporation of SCN^- ions into the crystal lattice of a tin perovskite to result in a three dimensional (3D) structure and thereby to improve the device performance and stability with suppressed recombination and enhanced tolerance to moisture.

Herein, the 3D tin perovskites incorporating thiocyanate with general chemical formula $FASnI_{(3-x)}(SCN)_x$, x = 0, 1, 2, or 3, were investigated for the first time through both experimental and theoretical approaches. For their applications as photovoltaic materials, the carbon-based mesostructured hole transporting material (HTM)-free device architecture was utilized.[25−28] The merit of this approach is highlighted as a manufacturing technique offering not only cheap but also large-scale processability.[6] PCE more than double compared to that of a control $FASnI_3$ device was obtained. Furthermore, the efficiency increased to 3.7% on incorporating phenethylammonium iodide (PEAI, 10%) and ethylenediammonium diiodide ($EDAI_2$, 5%) while preserving the moisture-tolerant properties. The new perovskite $FASnI(SCN)_2$ displayed greater device stability, even upon direct exposure to air, without being encapsulated within a hole-transport layer or a sealant, under ambient conditions.

EXPERIMENTAL SECTION

Perovskite solutions were prepared with precursors formamidinium iodide (FAI), formamidinium thiocyanate (FASCN), $Sn(SCN)_2$, SnI_2, and SnF_2 (10% mol ratio) in stoichiometric proportions and dissolved in dimethylformamide (DMF). These solutions of $FASnI_{3-x}(SCN)_x$ were stirred overnight near 23 °C. All resulting solutions based on SCN^- are yellow and stable, with no color change observed under a N_2 atmosphere over more than one year, implying no evident degradation. Utilizing the stable solutions, we adopted two annealing steps to prepare films by drop casting (DC), first at 65 °C for 20 min followed by annealing at 135 °C for 20 min for the formation of crystals. The resulting films displayed black color for x = 0−2, whereas a light pink color was observed for x = 3.

The triple mesoscopic HTM-free C electrodes were used for device fabrication. The electrodes were fabricated by spraying a compact layer of TiO_2 (thickness 40 nm) on etched FTO glass, followed by screen printing of a TiO_2 mesoporous layer (thickness 1 μm). This layer was annealed at 500 °C for 30 min. After annealing, Al_2O_3 (thickness 1 μm) and carbon (thickness ∼10 μm) layers were coated onto the TiO_2 layer via screen printing. Additionally, for devices with PEAI (10%), a NiO_x layer was screen-printed between alumina and carbon layers. The substrate was annealed at 400 °C for 30 min before use. The electrodes were transferred to a glovebox (N_2 environment, both O_2 and H_2O less than 10 ppm). The devices were fabricated via drop casting (DC). A precursor solution (1 M, 2.5 μL) prepared with the DMF solvent was dropped onto the electrode film at 65 °C. After the solution penetrated the carbon layer, the device was annealed at 135 °C for 20 min.

For the solvent extraction (SE) method, after solution penetration, the substrate was dipped in methyl phenyl ether and benzotrifluoride (equimolar mixture) for 15 min followed by annealing at 135 °C for 20 min. For the SE method with an $EDAI_2$ coadditive, $EDAI_2$ in varied proportions was added into a precursor solution with the DMF solvent. The remaining steps were the same as in the SE method.

RESULTS AND DISCUSSION

To garner a more detailed insight, we performed geometric optimizations of the crystal structures using the density functional theory (DFT) based on the Perdew−Burke−Ernzerhof (PBE) functional and plane-wave basis sets with a cutoff energy of 500 eV for $FASnI_{(3-x)}(SCN)_x$ (x = 0, 1, 2, or

https://dx.doi.org/10.1021/acsami.0c03704
ACS Appl. Mater. Interfaces XXXX, XXX, XXX−XXX

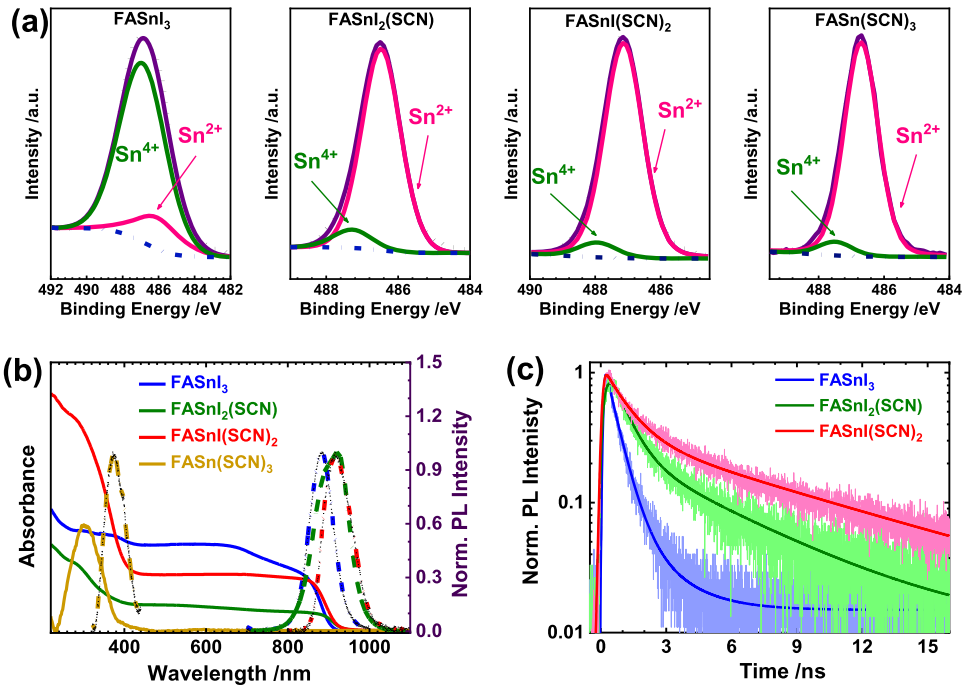

Figure 2. (a) XPS of Sn 3d recorded for fresh $FASnI_{(3-x)}(SCN)_x$ (x = 0–3) samples. The two lines deconvoluted from the measured spectra consist of Sn^{4+} lines (green) at slightly greater binding energies and Sn^{2+} lines (magenta). (b) Absorption (solid curves) and normalized photoluminescence (PL) (dashed curves) spectra of $FASnI_{(3-x)}(SCN)_x$ (x = 0–3) films deposited on quartz substrates controlled with precursors in stoichiometric proportions. (c) Normalized PL decay profiles of $FASnI_{(3-x)}(SCN)_x$ (x = 0–2) deposited on the glass substrate and measured using time-correlated single-photon counting (TCSPC).

3) perovskites; the corresponding optimized crystal structures are shown in Figure 1a. The calculated lattice parameters are summarized in Table S1, Supporting Information (SI). Perovskite $FASnI_3$ exhibits an orthorhombic crystal structure, whereas the replacement of iodide with thiocyanate leads to the formation of monoclinic and triclinic lattices. In the case of $FASnI_3$, our results are consistent with previous literature reports.[29] The optimized structures of SCN-based perovskites display remarkably decreased bond angles and bond lengths, as listed in Table S2, SI. The partial density of states (PDOS) for the perovskites is shown in Figure S1, SI. The valence band (VB) is composed mostly of I 5p orbitals; the conduction band (CB) is composed mainly of Sn 5p orbitals, in agreement with the results reported elsewhere.[29,30] Moreover, the substitution of SCN^- in perovskites increases the formation of energy relative to $FASnI_3$ and consequently imparts increased stability, as tabulated in Table S3, SI. As a strong correlation exists between the electric charge and the formation energy, we undertook a Bader charge analysis of $FASnI_{(3-x)}(SCN)_x$. For Sn^{2+} cations in $FASnI_{(3-x)}(SCN)_x$, the Bader oxidation states (Z) of Sn^{2+} were found to be 0.86, 1.05, 1.23, and 1.43 for x = 0–3, respectively. The numbers of Z for x = 2 and 3 were nearer to the Bader oxidation states for SnF_2 (1.56), indicating the trend of the formation of the Sn^{4+} species.[31,32] These results indicate a greater binding strength with the inclusion of SCN^- to feature increased stability relative to that of the pristine $FASnI_3$.

The effects of SCN^- on the $FASnI_{(3-x)}(SCN)_x$ crystal phase were experimentally investigated via Fourier transform infrared (FTIR) spectroscopy and X-ray diffraction (XRD). Our spectral results indicate an ambident nucleophilic nature of SCN^-, which serves as a bridging ligand to construct a stronger 3D network of octahedra.[33] The characteristic vibrational lines associated with the C≡N stretching vibrational mode of SCN^- were observed for all $FASnI_{(3-x)}(SCN)_x$ perovskites but not for x = 0 (Figures S2 and S3, SI; the corresponding sample preparations are presented in detail in the SI).[33] The IR spectra of the SCN-incorporating perovskites differed markedly from their precursors; red-shifted SCN^- vibrational lines were observed because of the partial donation of lone-pair electron density from the sulfur atom of the SCN^- group to a vacant orbital of the tin element, serving as solid evidence for the presence of thiocyanate in the core network of the perovskite structures.[34] The X-ray diffraction (XRD) patterns of $FASnI_{(3-x)}(SCN)_x$ perovskites (Figure 1b) were compared with those obtained from DFT calculations (Figure 1c). The main characteristic perovskite signals are located at ~14, ~28, and ~41° for x = 0–2 perovskites. They exhibit crystallinity with no residual precursor signal (Figure S4, SI). For x = 0–2, experimental and theoretical results matched well. For x = 3, the diffraction signals shifted gradually toward smaller angles because of an increase in lattice spacing (Table S2, SI). Furthermore, no undesired phase separation occurred, as indicated by the absence of precursor signals in both XRD patterns and IR spectra.[25] In lead-based perovskites, the inclusion of SCN^- transformed 3D perovskites into 2D structures,[22] but in our case, the small Sn^{2+} (cf. ionic radii of 103 and 122 pm for Sn^{2+} and Pb^{2+}, respectively) resulted in an appropriate octahedral factor while minimally altering the Goldschmidt tolerance factor because of the similar ionic radii of I^- and SCN^- (see Table S4, SI), thus preserving the 3D nature of the octahedron and corner-sharing capability of the $SnI_{6-x}(SCN)_x$ structures (Figure S2, SI). Additionally, two important characteristics of 2D perovskites, i.e., Bragg signals at small angles in XRD with 2θ less than 10° and an excitonlike peak in the UV–vis spectra of perovskite films, were absent,

https://dx.doi.org/10.1021/acsami.0c03704
ACS Appl. Mater. Interfaces XXXX, XXX, XXX–XXX

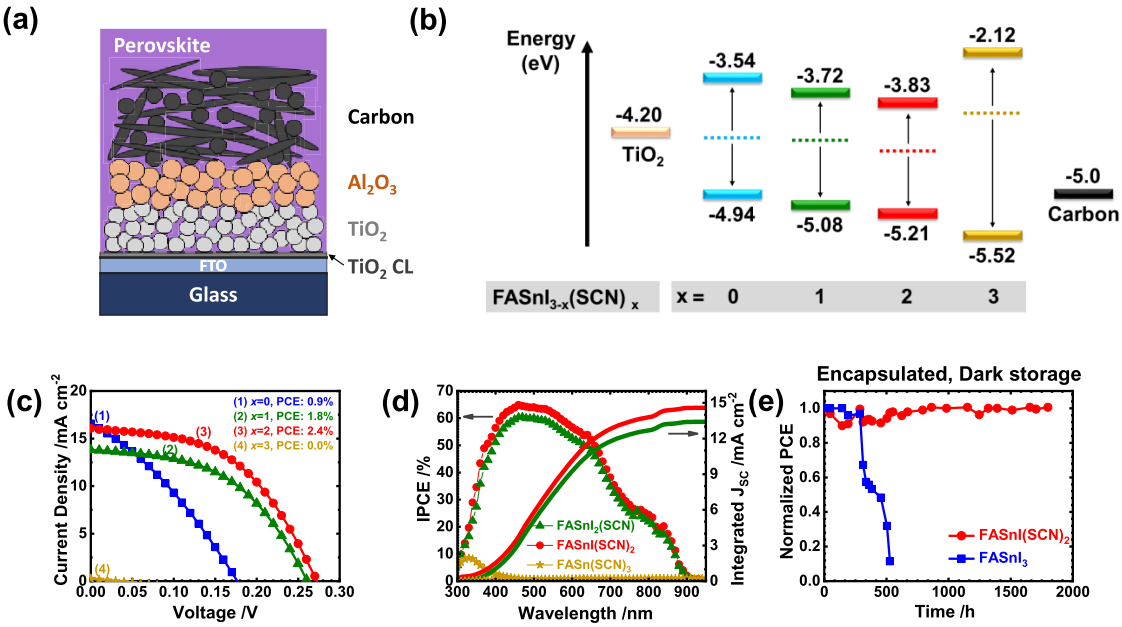

Figure 3. (a) Schematic representation of a mesoscopic TiO_2/Al_2O_3/carbon-based device. (b) Energy diagrams (energy/eV with respect to vacuum) of films with $FASnI_{(3-x)}(SCN)_x$ ($x = 0-3$). The positions of the work function (WF) are indicated with dashed lines for each species. (c) Representative $J-V$ characteristics of each $FASnI_{(3-x)}(SCN)_x$ ($x = 0-3$) device. (d) Representative IPCE spectra and integrated J_{sc} for the $x = 1-3$ devices. (e) Stability of the corresponding $FASnI_3$ and $FASnI(SCN)_2$ perovskite solar cells with encapsulation in an ambient environment with 65% relative humidity at 25 °C and stored in the dark.

hence confirming the formation of 3D structures for $FASnI_{(3-x)}(SCN)_x$ films.[35]

The chemical compositions of each perovskite were determined via X-ray photoelectron spectroscopy (XPS) and energy-dispersive X-ray spectroscopy (EDX); the results are shown in Figures S5 and S6, SI, respectively. The XPS survey scans of the XPS confirm that the S (1s) peak appeared when SCN was incorporated into the lattice structure (inset of Figure S5, SI). We quantified the Sn/S ratios in the bulk state with EDX spectra and those in the surface state with XPS survey scans of the tin perovskites; the results (Table S5, SI) showed that the Sn/S ratios matched satisfactorily for all of the $FASnI_{(3-x)}(SCN)_x$ films. Furthermore, Figure 2a shows the XPS spectra of Sn compositions for all four perovskite films. The evolution of Sn^{4+} lines on the surface of perovskites containing thiocyanate was greatly suppressed, indicative of a great tolerance to oxidation of tin. The Sn^{4+} ratios were only 9.0, 6.3, and 6.0% for $x = 1-3$, respectively; the corresponding proportions of Sn^{4+} were decreased in the bulk (plasma etching for 30 s) with only 5.8 ($x = 1$), 5.3 ($x = 2$), and 1.4% ($x = 3$). In contrast, $FASnI_3$ has 85.0% of Sn^{4+} on the surface and 36.9% in the bulk (Figure S7, SI). The suppressed oxidation of Sn^{2+} in perovskites containing thiocyanates is attributed to an increased hydrophobicity and strong binding, as confirmed by measurements of contact angles (Figure S8, SI), Bader charge analysis, and greater enthalpies of formation (Table S3, SI). These materials have hence the potential for improved photovoltaic performance, as indicated by their optimum band gaps, low Sn^{4+} concentrations, and strong binding characteristics.

Figure 2b shows the absorption and PL spectra of $FASnI_{(3-x)}(SCN)_x$ films on quartz substrates. The pristine $FASnI_3$ film shows a band gap of ~1.40 eV, whereas $FASnI_2(SCN)$ and $FASnI(SCN)_2$ have band gaps of 1.36 and 1.38 eV, respectively, which are smaller than that of $FASnI_3$. For $x = 1$ and $x = 2$, the binding energy of the I 5p orbitals is sufficiently high to hybridize with the S and N p orbitals, thereby maintaining a similar band gap compared to that of $FASnI_3$ with an only limited decrease of the valence bandwidth.[21] Furthermore, the pseudohalide has a small effect on decreasing the band gap because the Sn–I bond lengths are slightly increased (Table S2, SI) and this reduces the Sn s/I p hybridization strength, causing a downward shift of the conduction band minimum (CBM). Tin perovskite with $x = 3$, i.e., $FASn(SCN)_3$, is, however, a wide band gap semiconductor with a band gap of ~3.4 eV. This anomalous behavior for $FASn(SCN)_3$ is attributed to its distorted octahedral structure, short Sn–SCN bond lengths, and enhanced interaction of formamidinium (FA) molecular orbitals with the $Sn(SCN)_6$ matrix, causing an upward shift of the CBM levels and resulting in an increase in the band gap.[36] The energy level of the CBM is mostly influenced by the position of the Sn p orbital level that is shifted upward while increasing the SCN content. The complete replacement of I with SCN alters the bond lengths significantly. Most likely, this is a confinement effect, i.e., as the Sn–X distances decrease drastically in the case of $FASn(SCN)_3$ (Table S2, SI), an electron on the Sn atom becomes more confined and its energy increases. Furthermore, the Sn s/X p hybridization strength increases to some extent due to the shorter bond lengths. This results in a tighter cage around the cation, reducing the polarizability of the perovskite. The reduced polarizability results in a subsequently higher band gap that is evident in the case of $FASn(SCN)_3$ with the upward shift of the CBM. Similar trends were also observed based on the ultraviolet photoelectron spectra (UPS) data reported for other systems.[31,32]

We performed PL decay experiments with time-correlated single-photon counting (TCSPC); the resulting temporal profiles are shown in Figure 2c. The PL transients were fitted

https://dx.doi.org/10.1021/acsami.0c03704
ACS Appl. Mater. Interfaces XXXX, XXX, XXX–XXX

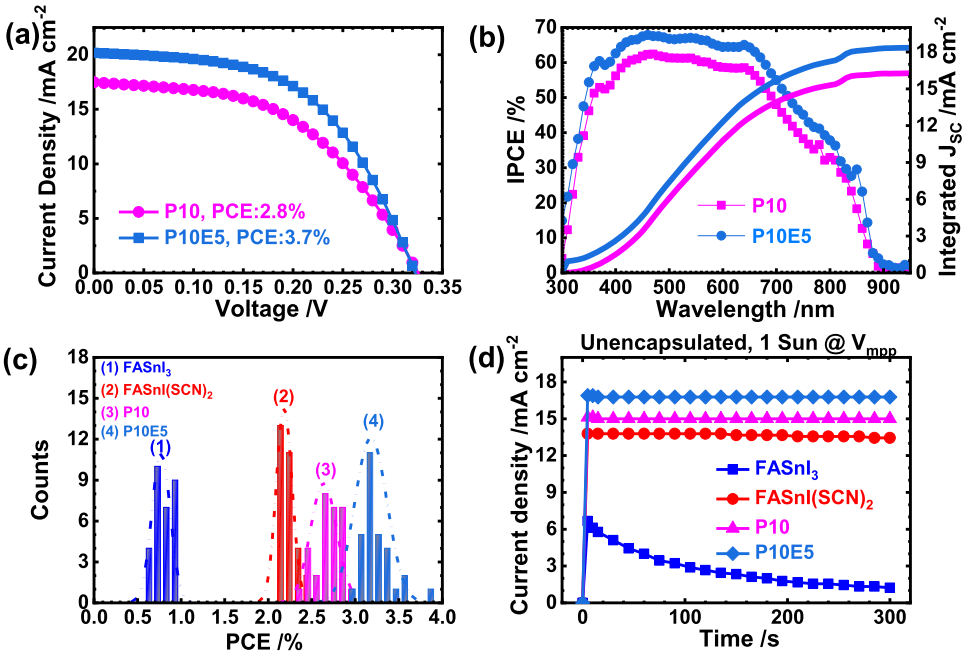

Figure 4. (a) Current−voltage curves of P10 and P10E5 devices with PCEs of 2.8 and 3.7%, respectively. (b) Corresponding IPCE spectra and integrated J_{sc} of P10 and P10E5 devices. (c) Histograms of 30 fresh devices fabricated under the same experimental conditions as those for $FASnI_3$, $FASnI(SCN)_2$, P10, and P10E5 devices. (d) Steady current densities measured at the point of the maximum power of unencapsulated $FASnI_3$, $FASnI(SCN)_2$, P10, and P10E5 devices under 1 sun irradiation (AM1.5G solar simulator) for 300 s under ambient conditions with ~65% RH.

using biexponential decay components; Table S6, SI, summarizes the corresponding lifetimes and relative amplitudes. The first (τ_1) and second (τ_2) components are associated with a nonradiative surface-state relaxation and the bulk recombination of perovskites, respectively. With an increase in thiocyanate content, τ_1 increases and the associated amplitude decreases, denoting decreased nonradiative surface-state relaxation. Moreover, τ_2 increased with an increase in x; the average τ_{PL} increased from 0.76 ns for $FASnI_3$ to 2.92 and 5.94 ns for $FASnI_2(SCN)$ and $FASnI(SCN)_2$, respectively. These results show the trend of retarded charge recombination for increasing the number of SCN^- in the tin perovskites. Therefore, the pseudohalide replacement helps the tin perovskites to decrease the defect states and suppress the Sn^{2+}/Sn^{4+} oxidation, which is consistent with the XPS and DFT results. A similar phenomenon on defect-state passivation was also reported for Pb perovskites incorporating SCN.[37]

Because of the large contact angles for the precursor solutions involving SCN, the corresponding $FASnI_{3-x}(SCN)_x$ films (x = 1−3) showed poor morphologies (Figure S9, SI). Therefore, the planar heterojunction-type solar-cell device cannot be fabricated with satisfactory performance. All devices were thus fabricated according to a mesoporous carbon electrode structure shown in Figure 3a. Mesoporous TiO_2, Al_2O_3, and carbon layers were screen-printed on a glass/FTO/c-TiO_2 substrate layer by layer. The perovskite precursor solution was then dropped onto the surface of the carbon layer to infiltrate into the triple layers through the mesoporous films. The cross-sectional SEM images of the $FASnI_{3-x}(SCN)_x$ PSC are presented in Figure S10, SI. The perovskites penetrated well into the pores of the entire TiO_2 layer. The boundary between m-TiO_2/perovskite and Al_2O_3/perovskite is indistinct because of the excellent infiltration of the perovskite. Figure 3b shows an energy-level diagram of the $FASnI_{3-x}(SCN)_x$ PSC. The valence band maxima (VBM) of these perovskites were deduced from their ionization energies obtained from ultraviolet photoelectron spectra (UPS) (Figure S11, SI); the conduction band minima (CBM) were calculated accordingly from their band gaps and VBM values, as shown in Figure 3b. The substitution of SCN^- in the $FASnI_{3-x}(SCN)_x$ films plays a significant role in modulating both the CBM and VBM levels, similarly to other mixed-halide systems.[7,38] Trends similar to those of other mixed-halide systems were observed for the work functions deduced from the UPS measurements.[39] The decrease of the energy levels of the VBM upon inclusion of SCN^- has further implications for the stability of the perovskites because of the tendency of the materials to undergo oxidative degradation.[40]

Figure 3c shows the current density vs voltage (J−V) curves of the fabricated PSC measured under AM1.5G 1 sun illumination (100 mW cm^{-2}) in the reverse scan/forward bias mode; the corresponding photovoltaic parameters are listed in Table S7, SI. The best $FASnI(SCN)_2$ PSC (x = 2) exhibited PCE 2.4%. This PCE is almost three times that of the $FASnI_3$ device (PCE = 0.9%), for which the efficiency of the $FASnI_3$ cell is similar to those reported elsewhere.[27,41] The best x = 2 solar cell displays a negligible hysteresis in the J−V curves (Figure S12, SI). The greater offset between the VBM of the perovskite and the carbon electrode can lead to thermionic losses that might cause a loss of the open-circuit potential in solar cell devices, as evident in the cases of x = 0 and 3.[40] The IPCE spectra of PSC corresponding to x = 1−3 measured in air are shown in Figure 3d. The IPCE for $FASnI_3$ was not measurable because of the rapid degradation of the perovskite through oxidation, which we observed previously.[27] The IPCE plots of $FASnI_{3-x}(SCN)_x$ (x = 1, 2, or 3) resemble the absorption spectra of the corresponding perovskites with maxima IPCE values attaining ~60% near 450 nm for x = 1 and 2. The integrated currents extracted from IPCE are also consistent with the experimental J_{sc}. As expected, a plot with

https://dx.doi.org/10.1021/acsami.0c03704
ACS Appl. Mater. Interfaces XXXX, XXX, XXX−XXX

small IPCE values (Figure 3d) covering a narrow region at large energy was obtained in the case of $FASn(SCN)_3$ because of its wide band gap. For the stability test, the encapsulated $FASnI(SCN)_2$ device stored under ambient conditions (RH = 65%) in the dark maintained nearly identical performance for nearly 2000 h, whereas pristine $FASnI_3$ devices degraded to nearly zero within 500 h, indicating the superior long-term ambient storage stability with thiocyanate incorporation (Figure 3e). The ambient aging of the precursor solutions had no effect on the performance of the $FASnI(SCN)_2$ device but severely affected that of the pristine $FASnI_3$ device (Figure S13 and Table S8, SI). This result indicates that ambient storage of tin perovskite precursor solutions for cheap and scalable production of tin-based PSCs is feasible. Furthermore, we performed accelerated stability tests by exposing $FASnI_3$ and $FASnI(SCN)_2$ films to ambient conditions and performing XRD and XPS. No degradation occurred for $FASnI(SCN)_2$, whereas some precursor signals appeared in the $FASnI_3$ XRD patterns, which indicated considerable degradation for $FASnI_3$ (Figure S14, SI). To measure Sn 3d XPS spectra, we exposed films to air for 15 h. Even after exposure to air, the $FASnI(SCN)_2$ film showed an insignificant concentration of Sn^{4+}, whereas the $FASnI_3$ film showed complete degradation (Figure S15, SI). These results revealed that the stability of the tin-based perovskite was improved upon introducing pseudohalide SCN^-, as reported for the $FASnI(SCN)_2$ device.

To boost the performance of the $FASnI(SCN)_2$ device, we incorporated 10% phenethylammonium iodide (PEAI) as a dopant, because the latter is broadly used to enhance crystallinity, to suppress trap-assisted charge recombination, decrease the background carrier density, and enhance the stability for a tin perovskite.[10,42−45] The resulting structure $PEA_{0.1}FA_{0.9}SnI(SCN)_2$, based on the stoichiometric ratio, is denoted P10. The addition of PEA^+ might form a 2D/3D crystal structure and improve crystallinity, as realized from the XRD spectra shown in Figures S16, SI. However, a slight blue shift by ∼20 nm was observed in both absorption and PL spectra with the incorporation of 10% PEAI (Figure S17, SI), indicating the incorporation of the PEA cation inside the crystal structure. The P10 device fabricated with a glass/FTO/c-TiO_2/mp-TiO_2/Al_2O_3/C structure using the drop casting (DC) method showed poorer PCE, ∼2.0%. An additional NiO_x layer was hence introduced between the alumina and carbon layers for improved extraction of holes because P10 has a more deeply lying VBM, as shown in Figure S18, SI, for the corresponding energy levels of each layer and the device structure. This strategy further improved the PCE of the P10 device to 2.4% (Figure S19, SI). We applied a two-step solvent extraction (SE) method, resulting in controllable crystal growth and hence improving the performance to attain a PCE of 2.8% (Figure 4a).[27,28] Although the devices fabricated using the SE method showed larger V_{OC} than those using the DC method, J_{SC} was only slightly improved.

To enhance the PCE of the P10 device using the SE method, we added $EDAI_2$ in varied proportions, as reported elsewhere.[46] $EDAI_2$ became a coadditive in the P10 precursor solution with the $EDAI_2$ proportions varying from 0 to 7%; the best device performance was obtained with 5% $EDAI_2$ (denoted P10E5). The resulting PV parameters of the P10 devices with varied $EDAI_2$ proportions are presented in Figure S20, SI. The best P10E5 device featured J_{SC} = 20.17 mA cm^{-2}, V_{OC} = 322 mV, fill factor (FF) = 0.574, and overall PCE = 3.7%. The current−voltage curves of the best P10E5 and P10 devices are shown in Figure 4a; the corresponding IPCE plots are shown in Figure 4b. The best P10E5 solar cell displayed a negligible hysteresis in the $J-V$ curves (Figure S21, SI). Figure 4c shows the histograms for 30 devices made of $FASnI_3$, $FASnI(SCN)_2$, P10, and P10E5; the corresponding photovoltaic parameters are summarized in Table S9, SI. From the statistical boxplot (Figure S22 and Tables S10 and S13, SI), we observed that the incorporation of thiocyanate pseudohalide effectively improves the device performance relative to that of the control device ($FASnI_3$). This enhancement was due mainly to the significantly increased V_{oc} and FF, to be clarified with further characterization.

We undertook systematic investigations to understand the superior performance of the P10E5 device. As shown by the XRD data in Figure S16, SI, the addition of PEAI and $EDAI_2$ improved the overall crystallinity compared to that of the pristine $FASnI(SCN)_2$ perovskite. Both P10 and P10E5 devices exhibited effective penetration, according to the SEM cross-sectional images shown in Figure S23, SI. Devices made of P10 and P10E5 exhibited superior charge transfer and suppressed charge recombination relative to those of the pristine $FASnI(SCN)_2$ and $FASnI_3$ devices, as shown in the Nyquist plots (Figure S24 and Table S14, SI). Further insight was obtained from V_{OC} and J_{SC} characteristics dependent on the light intensity, as shown in Figure S25, SI. All thiocyanate-containing tin perovskites exhibited smaller slopes (ideality factor) than that of $FASnI_3$ in the semilog plots of V_{oc} vs light intensity, indicating suppressed charge recombination. Moreover, a log plot of the variation of J_{SC} with light intensity yielded slopes nearer unity, indicating a suppressed bimolecular recombination, i.e., fewer hole-trap states. These fewer hole-trap states decreased the accumulation of holes and the building up of positive space charge at the interface; negligible space charge effects consequently resulted in improved device performances.[47]

For $FASnI_3$, $FASnI(SCN)_2$, P10, and P10E5 devices, we performed an accelerated stability test for unencapsulated devices with continuous illumination in an ambient atmosphere under the condition of the point of maximum power with no bias. As displayed in Figure 4d and S26a, SI, the pristine $FASnI_3$ device showed a rapid loss of efficiency within 2 min, whereas the other devices with SCN^- maintained the same performance for more than 5 min with no significant degradation. For the stability tests in the dark under ambient conditions without the encapsulation of the cells, only a slightly degraded PCE was observed for the P10E5 device, whereas the efficiency of the $FASnI_3$ device decreased to zero in a few minutes (Figure S26b and Table S15, SI). Remarkably, as in a mesostructured carbon-based device architecture, the mesopores of carbon readily allowed the diffusion of oxygen and gaseous molecular water; the great device stability remained even upon exposure to air with no additional protection from HTM or metal-electrode layers.[48] The slight degradation of our unencapsulated P10E5 device under severe ambient conditions is remarkable compared with the tin-based PSC reported elsewhere.[27,46] One possibility for the observed great moisture stability of the unencapsulated P10E5 device is the hydrophobicity of the device surface. For this reason, we measured the contact angles for water dropped on the devices made of $FASnI_3$, $FASnI(SCN)_2$, P10, and P10E5 (Figure S27, SI). The contact angle of a blank mesoporous C-based device was only 32°, but that on a $FASnI_3$ device increased to 59°; the contact angles for devices with thiocyanate increased to 83° for

https://dx.doi.org/10.1021/acsami.0c03704
ACS Appl. Mater. Interfaces XXXX, XXX, XXX−XXX

$FASnI(SCN)_2$ and 91° for both P10 and P10E5 devices. We hence demonstrated that the involvement of a pseudohalide in tin perovskites increases moisture tolerance because of the hydrophobic property of device surfaces.

CONCLUSIONS

In conclusion, herein, we incorporated a thiocyanate anion to produce tin perovskites in a new series, $FASnI_{3-x}(SCN)_x$ (x = 0−3), based on both experimental and theoretical approaches. Thiocyanate provides great tolerance to moisture and oxygen because of its hydrophobic property and tendency of charge delocalization that efficiently suppresses the formation of Sn^{4+} defects to form robust, reproducible, and high-performance tin perovskite solar cells. Our calculations show that substituting SCN^- for iodide significantly affects the lattice parameters, increases the formation energy of the perovskites, and tunes the band gap, hence demonstrating that stable tin perovskites can be produced by substituting thiocyanate ions for iodide. This incorporation of thiocyanate in tin perovskites promotes the rapid transport of charge carriers by depressing the nonradiative process and retarding the charge recombination. The $FASnI(SCN)_2$ device in the presence of PEAI (10%) and $EDAI_2$ (5%) as coadditives attained a PCE of 3.7%, which is almost four times than that of the pristine $FASnI_3$ device, accompanied by excellent moisture tolerance, strong light soaking, and long-term stability.

ASSOCIATED CONTENT

Supporting Information

The Supporting Information is available free of charge at https://pubs.acs.org/doi/10.1021/acsami.0c03704.

Details about materials, characterizations, DFT calculations, simulated projected density of states, DFT-simulated crystal structure, FTIR spectra, thin-film XRD patterns, XPS survey scan, EDX spectra, XPS spectra of Sn 3d, water contact angle, top-view SEM images, SEM cross-sectional images, UPS, $J-V$ characteristics, photovoltaic performance, XRD test of stability, thin-film XRD patterns, absorption and normalized PL spectra, energy diagrams, box-plot statistical distribution, Nyquist plots, dependence on the light intensity, and photovoltaic performance stability (PDF)

AUTHOR INFORMATION

Corresponding Authors

Chen-Hsiung Hung − *Institute of Chemistry, Academia Sinica, Nankang, Taipei 11529, Taiwan*; Email: chhung@gate.sinica.edu.tw

Eric Wei-Guang Diau − *Department of Applied Chemistry and Institute of Molecular Science and Center for Emergent Functional Matter Science, National Chiao Tung University, Hsinchu 30010, Taiwan*; orcid.org/0000-0001-6113-5679; Email: diau@mail.nctu.edu.tw

Authors

Mohammad Rameez − *Department of Applied Chemistry and Institute of Molecular Science, National Chiao Tung University, Hsinchu 30010, Taiwan; Institute of Chemistry and Sustainable Chemical Science and Technology (SCST), Taiwan International Graduate Program (TIGP), Academia Sinica, Nankang, Taipei 11529, Taiwan*; orcid.org/0000-0003-4712-9584

Eric Yan-Ru Lin − *Department of Applied Chemistry and Institute of Molecular Science, National Chiao Tung University, Hsinchu 30010, Taiwan*

Putikam Raghunath − *Department of Applied Chemistry and Institute of Molecular Science, National Chiao Tung University, Hsinchu 30010, Taiwan*

Sudhakar Narra − *Department of Applied Chemistry and Institute of Molecular Science, National Chiao Tung University, Hsinchu 30010, Taiwan*

Donghoon Song − *Department of Applied Chemistry and Institute of Molecular Science, National Chiao Tung University, Hsinchu 30010, Taiwan*; orcid.org/0000-0003-0914-1507

Ming-Chang Lin − *Department of Applied Chemistry and Institute of Molecular Science and Center for Emergent Functional Matter Science, National Chiao Tung University, Hsinchu 30010, Taiwan*; orcid.org/0000-0003-3963-6017

Complete contact information is available at: https://pubs.acs.org/10.1021/acsami.0c03704

Notes

The authors declare no competing financial interest.

ACKNOWLEDGMENTS

Taiwan Ministry of Science and Technology (MOST) provided financial support to this research (MOST 105-2119-M-009-011-MY3, MOST 107-2119-384 M-009-001, and MOST 108-2119-M-009-004). This work was also financially supported by the Center for Emergent Functional Matter Science of National Chiao Tung University through The Featured Areas Research Center Program within the framework of the Higher Education SPROUT Project by Taiwan Ministry of Education (MOE). National Synchrotron Radiation Research Center (NSRRC), Hsinchu Science Park, Taiwan, provided beam time for measurements of ultraviolet photoelectron spectra.

REFERENCES

(1) NREL. Best Research-Cell Efficiency Chart, Photovoltaic Research. 2020, https://www.nrel.gov/pv/cell-efficiency.html.

(2) Ke, W.; Kanatzidis, M. G. Prospects for Low-Toxicity Lead-Free Perovskite Solar Cells. *Nat. Commun.* **2019**, *10*, No. 965.

(3) Diau, E. W.-G.; Jokar, E.; Rameez, M. Strategies To Improve Performance and Stability for Tin-Based Perovskite Solar Cells. *ACS Energy Lett.* **2019**, *4*, 1930−1937.

(4) Kim, H.; Lee, Y. H.; Lyu, T.; Yoo, J. H.; Park, T.; Oh, J. H. Boosting the Performance and Stability of Quasi-Two-Dimensional Tin-Based Perovskite Solar Cells Using the Formamidinium Thiocyanate Additive. *J. Mater. Chem. A* **2018**, *6*, 18173−18182.

(5) Wang, R.; Wang, J.; Tan, S.; Duan, Y.; Wang, Z. K.; Yang, Y. Opportunities and Challenges of Lead-Free Perovskite Optoelectronic Devices. *Trends Chem.* **2019**, *1*, 368−379.

(6) Chen, H.; Yang, S. Methods and Strategies for Achieving High-Performance Carbon-Based Perovskite Solar Cells without Hole Transport Materials. *J. Mater. Chem. A* **2019**, *7*, 15476−15490.

(7) Konstantakou, M.; Stergiopoulos, T. A Critical Review on Tin Halide Perovskite Solar Cells. *J. Mater. Chem. A* **2017**, *5*, 11518−11549.

(8) Tai, Q.; Guo, X.; Tang, G.; You, P.; Ng, T.-W.; Shen, D.; Cao, J.; Liu, C.-K.; Wang, N.; Zhu, Y.; Lee, C. S.; et al. Antioxidant Grain Passivation for Air-Stable Tin-Based Perovskite Solar Cells. *Angew. Chem., Int. Ed.* **2019**, *58*, 806−810.

(9) Jokar, E.; Chien, C.-H.; Tsai, C.-M.; Fathi, A.; Diau, E. W.-G. Robust Tin-Based Perovskite Solar Cells with Hybrid Organic Cations to Attain Efficiency Approaching 10%. *Adv. Mater.* **2019**, *31*, No. 1804835.

(10) Horn, J.; Scholz, M.; Oum, K.; Lenzer, T.; Schlettwein, D. Influence of Phenylethylammonium Iodide as Additive in the Formamidinium Tin Iodide Perovskite on Interfacial Characteristics and Charge Carrier Dynamics. *APL Mater.* **2019**, *7*, No. 031112.
(11) Li, F.; Zhang, C.; Huang, J.-H.; Fan, H.; Wang, H.; Wang, P.; Zhan, C.; Liu, C.-M.; Li, X.; Yang, L.-M.; Song, Y.; et al. A Cation-Exchange Approach for the Fabrication of Efficient Methylammonium Tin Iodide Perovskite Solar Cells. *Angew. Chem., Int. Ed.* **2019**, *58*, 6688−6692.
(12) Xie, G.; Xu, L.; Sun, L.; Xiong, Y.; Wu, P.; Hu, B. Insight into the Reaction Mechanism of Water, Oxygen and Nitrogen Molecules on a Tin Iodine Perovskite Surface. *J. Mater. Chem. A* **2019**, *7*, 5779−5793.
(13) Liu, J.; Shi, J.; Li, D.; Zhang, F.; Li, X.; Xiao, Y.; Wang, S. Molecular Design and Photovoltaic Performance of a Novel Thiocyanate-Based Layered Organometal Perovskite Material. *Synth. Met.* **2016**, *215*, 56−63.
(14) Numata, Y.; Sanehira, Y.; Ishikawa, R.; Shirai, H.; Miyasaka, T. Thiocyanate Containing Two-Dimensional Cesium Lead Iodide Perovskite, Cs2PbI2(SCN)2: Characterization, Photovoltaic Application, and Degradation Mechanism. *ACS Appl. Mater. Interfaces* **2018**, *10*, 42363−42371.
(15) Yang, S.; Liu, W.; Zuo, L.; Zhang, X.; Ye, T.; Chen, J.; Li, C.-Z.; Wu, G.; Chen, H. Thiocyanate Assisted Performance Enhancement of Formamidinium Based Planar Perovskite Solar Cells through a Single One-Step Solution Process. *J. Mater. Chem. A* **2016**, *4*, 9430−9436.
(16) Halder, A.; Chulliyil, R.; Subbiah, A. S.; Khan, T.; Chattoraj, S.; Chowdhury, A.; Sarkar, S. K. Pseudohalide (SCN−)-Doped MAPbI3 Perovskites: A Few Surprises. *J. Phys. Chem. Lett.* **2015**, *6*, 3483−3489.
(17) Jiang, Q.; Rebollar, D.; Gong, J.; Piacentino, E. L.; Zheng, C.; Xu, T. Pseudohalide-Induced Moisture Tolerance in Perovskite CH3NH3Pb(SCN)2I Thin Films. *Angew. Chem., Int. Ed.* **2015**, *54*, 7617−7620.
(18) Liu, X.; Huang, K. L.; Liang, G. M.; Wang, M. S.; Guo, G. C. Molecular Design of Luminescent Halogeno-Thiocyano-d 10 Metal Complexes with in Situ Formation of the Thiocyanate Ligand. *CrystEngComm* **2009**, *11*, 1615−1620.
(19) Labram, J. G.; Venkatesan, N. R.; Takacs, C. J.; Evans, H. A.; Perry, E. E.; Wudl, F.; Chabinyc, M. L. Charge Transport in a Two-Dimensional Hybrid Metal Halide Thiocyanate Compound. *J. Mater. Chem. C* **2017**, *5*, 5930−5938.
(20) Walker, B.; Kim, G.; Kim, J. Y. Pseudohalides in Lead-Based Perovskite Semiconductors. *Adv. Mater.* **2019**, *31*, No. 1807029.
(21) Ganose, A. M.; Savory, C. N.; Scanlon, D. O. Electronic and Defect Properties of (CH3NH3)2Pb(SCN)2I2 Analogues for Photovoltaic Applications. *J. Mater. Chem. A* **2017**, *5*, 7845−7853.
(22) Daub, M.; Hillebrecht, H. Synthesis, Single-Crystal Structure and Characterization of (CH3NH3)2Pb(SCN)2I2. *Angew. Chem., Int. Ed.* **2015**, *54*, 11016−11017.
(23) Clavijo Penagos, J. I.; Romero, E. R.; Gordillo, G.; Correa Hoyos, J. M.; Reinoso Sánchez, M. Á. On the True Band Gap of the (CH3NH3)2Pb(SCN)2I2 Hybrid Perovskite: An Interesting Solar-Cell Material. *Phys. Status Solidi RRL* **2018**, *12*, No. 1700376.
(24) Wang, F.; Jiang, X.; Chen, H.; Shang, Y.; Liu, H.; Wei, J.; Zhou, W.; He, H.; Liu, W.; Ning, Z. 2D-Quasi-2D-3D Hierarchy Structure for Tin Perovskite Solar Cells with Enhanced Efficiency and Stability. *Joule* **2018**, *2*, 2732−2743.
(25) Tsai, C.-M.; Mohanta, N.; Wang, C.-Y.; Lin, Y.-P.; Yang, Y.-W.; Wang, C.-L.; Hung, C.-H.; Diau, E. W.-G. Formation of Stable Tin Perovskites Co-Crystallized with Three Halides for Carbon-Based Mesoscopic Lead-Free Perovskite Solar Cells. *Angew. Chem., Int. Ed.* **2017**, *56*, 13819−13823.
(26) Tsai, C.-M.; Wu, G.-W.; Narra, S.; Chang, H.-M.; Mohanta, N.; Wu, H.-P.; Wang, C.-L.; Diau, E. W.-G. Control of Preferred Orientation with Slow Crystallization for Carbon-Based Mesoscopic Perovskite Solar Cells Attaining Efficiency 15%. *J. Mater. Chem. A* **2017**, *5*, 739−747.
(27) Tsai, C.-M.; Lin, Y.-P.; Krishna Pola, M.; Narra, S.; Jokar, E.; Yang, Y.-W.; Diau, E. W.-G. Control of Crystal Structures and Optical Properties with Hybrid Formamidinium and 2-Hydroxyethylammonium Cations for Mesoscopic Carbon-Electrode Tin-Based Perovskite Solar Cells. *ACS Energy Lett.* **2018**, *3*, 2077−2085.
(28) Chan, C. Y.; Wang, Y.; Wu, G. W.; Diau, E. W.-G. Solvent-Extraction Crystal Growth for Highly Efficient Carbon-Based Mesoscopic Perovskite Solar Cells Free of Hole Conductors. *J. Mater. Chem. A* **2016**, *4*, 3872−3878.
(29) Shi, T.; Zhang, H.-S.; Meng, W.; Teng, Q.; Liu, M.; Yang, X.; Yan, Y.; Yip, H.-L.; Zhao, Y.-J. Effects of Organic Cations on the Defect Physics of Tin Halide Perovskites. *J. Mater. Chem. A* **2017**, *5*, 15124−15129.
(30) Bernal, C.; Yang, K. First-principles Hybrid Functional Study of the Organic−inorganic Perovskites CH3NH3SnBr3 and CH3NH3SnI3. *J. Phys. Chem. C* **2014**, *118*, 24383−24388.
(31) Yamamoto, K.; Iikubo, S.; Yamasaki, J.; Ogomi, Y.; Hayase, S. Structural Stability of Iodide Perovskite: A Combined Cluster Expansion Method and First-principles Study. *J. Phys. Chem. C* **2017**, *121*, 27797−27804.
(32) Xiao, Z.; Lei, H.; Zhang, X.; Zhou, Y.; Hosono, H.; Kamiya, T. Ligand-Hole in [SnI6] Unit and Origin of Band Gap in Photovoltaic Perovskite Variant Cs2SnI6. *Bull. Chem. Soc. Jpn.* **2015**, *88*, 1250−1255.
(33) Chamberlain, B. R.; Moser, W. Tin (II) Thiocyanate and Complex Thiocyanates. *J. Chem. Soc., A* **1969**, 354−358.
(34) Holt, M. S.; Wilson, W. L.; Nelson, J. H. Transition Metal-yin Chemistry. *Chem. Rev.* **1989**, *89*, 11−49.
(35) Li, C.-H.; Tsai, C.-C.; Liao, M.-Y.; Su, Y.-A.; Lin, S.-T.; Chueh, C.-C. Stable, Color-Tunable 2D SCN-Based Perovskites: Revealing the Critical Influence of an Asymmetric Pseudo-Halide on Constituent Ions. *Nanoscale* **2019**, *11*, 2608−2616.
(36) Jong, U. G.; Yu, C. J.; Jang, Y. M.; Ri, G. C.; Hong, S. N.; Pae, Y. H. Revealing the Stability and Efficiency Enhancement in Mixed Halide Perovskites MAPb(I1−xClx)3 with Ab-initio Calculations. *J. Power Sources* **2017**, *350*, 65−72.
(37) Tai, Q.; You, P.; Sang, H.; Liu, Z.; Hu, C.; Chan, H. L. W.; Yan, F. Efficient and Stable Perovskite Solar Cells Prepared in Ambient Air Irrespective of the Humidity. *Nat. Commun.* **2016**, *7*, No. 11105.
(38) Hao, F.; Stoumpos, C. C.; Cao, D. H.; Chang, R. P. H.; Kanatzidis, M. G. Lead-free Solid-state Organic−inorganic Halide Perovskite Solar Cells. *Nat. Photonics* **2014**, *8*, 489−494.
(39) Bi, C.; Shao, Y.; Yuan, Y.; Xiao, Z.; Wang, C.; Gao, Y.; Huang, J. Understanding the Formation and Evolution of Interdiffusion Grown Organolead Halide Perovskite Thin Films by Thermal Annealing. *J. Mater. Chem. A* **2014**, *2*, 18508−18514.
(40) Zhao, Z.; Gu, F.; Li, Y.; Sun, W.; Ye, S.; Rao, H.; Liu, Z.; Bian, Z.; Huang, C. Mixed-Organic-Cation Tin Iodide for Lead-free Perovskite Solar Cells with Efficiency 8.12%. *Adv. Sci.* **2017**, *4*, No. 1700204.
(41) Rameez, M.; Shahbazi, S.; Raghunath, P.; Lin, M. C.; Hung, C. H.; Diau, E. W.-G. Development of Novel Mixed Halide/Superhalide Tin-Based Perovskites for Mesoscopic Carbon-Based Solar Cells. *J. Phys. Chem. Lett.* **2020**, *11*, 2443−2448.
(42) Liao, Y.; Liu, H.; Zhou, W.; Yang, D.; Shang, Y.; Shi, Z.; Li, B.; Jiang, X.; Zhang, L.; Quan, L. N.; Quintero-Bermudez, R.; et al. Highly Oriented Low-dimensional Tin Halide Perovskites with Enhanced Stability and Photovoltaic Performance. *J. Am. Chem. Soc.* **2017**, *139*, 6693−6699.
(43) Shao, S.; Dong, J.; Duim, H.; ten Brink, G. H.; Blake, G. R.; Portale, G.; Loi, M. A. Enhancing the Crystallinity and Perfecting the Orientation of Formamidinium Tin Iodide for Highly Efficient Sn-Based Perovskite Solar Cells. *Nano Energy* **2019**, *60*, 810−816.
(44) Rath, T.; Handl, J.; Weber, S.; Friesenbichler, B.; Fürk, P.; Troi, L.; Dimopoulos, T.; Kunert, B.; Resel, R.; Trimmel, G. Photovoltaic Properties of a Triple Cation Methylammonium/Formamidinium/Phenylethylammonium Tin Iodide Perovskite. *J. Mater. Chem. A* **2019**, *7*, 9523−9529.
(45) Tai, Q.; Cao, J.; Wang, T.; Yan, F. Recent Advances toward Efficient and Stable Tin-based Perovskite Solar Cells. *EcoMat* **2019**, *1*, No. e12004.

https://dx.doi.org/10.1021/acsami.0c03704
ACS Appl. Mater. Interfaces XXXX, XXX, XXX−XXX

(46) Jokar, E.; Chien, C.-H.; Fathi, A.; Rameez, M.; Chang, Y.-H.; Diau, E. W.-G. Slow Surface Passivation and Crystal Relaxation with Additives to Improve Device Performance and Durability for Tin-based Perovskite Solar Cells. *Energy Environ. Sci.* **2018**, *11*, 2353−2362.
(47) Tress, W.; Yavari, M.; Domanski, K.; Yadav, P.; Niesen, B.; Correa Baena, J. P.; Hagfeldt, A.; Graetzel, M. Interpretation and Evolution of Open-circuit Voltage, Recombination, Ideality Factor and Subgap Defect States during Reversible Light-soaking and Irreversible Degradation of Perovskite Solar Cells. *Energy Environ. Sci.* **2018**, *11*, 151−165.
(48) Fagiolari, L.; Bella, F. Carbon-Based Materials for Stable, Cheaper and Large-scale Processable Perovskite Solar Cells. *Energy Environ. Sci.* **2019**, *12*, 3437−3472.

https://dx.doi.org/10.1021/acsami.0c03704
ACS Appl. Mater. Interfaces XXXX, XXX, XXX−XXX